Correspondence to:
B. Huai,
huaibaojuan@126.com

Author Contributions:
Data curation: Brice Noël
Formal analysis: Baojuan Huai, Michiel R. van den Broeke, Carleen H. Reijmer, Brice Noël
Funding acquisition: Michiel R. van den Broeke
Methodology: Baojuan Huai, Michiel R. van den Broeke, Carleen H. Reijmer, Brice Noël
Supervision: Michiel R. van den Broeke, Carleen H. Reijmer
Writing – original draft: Baojuan Huai
Writing – review & editing: Michiel R. van den Broeke, Carleen H. Reijmer, Brice Noël

A Daily 1-km Resolution Greenland Rainfall Climatology (1958–2020) From Statistical Downscaling of a Regional Atmospheric Climate Model

Baojuan Huai[1] , Michiel R. van den Broeke[2] , Carleen H. Reijmer[2] , and Brice Noël[2]

[1]College of Geography and Environment, Shandong Normal University, Jinan, China, [2]Institute for Marine and Atmospheric Research, Utrecht University, Utrecht, The Netherlands

Abstract A daily, gridded 1-km rainfall climatology (1958–2020) for Greenland is presented, including the Greenland ice sheet (GrIS), the peripheral glaciers and ice caps (GIC), and ice-free tundra. It is obtained by statistically downscaling the 5.5 km output of the regional atmospheric climate model version 2 to a resolution of 1 km, using the elevation dependence of snowfall fraction. Based on this new product, the average total annual rainfall in Greenland during 1958–2020 is estimated to be 111.4 ± 11.2 Gt/year, of which 28.6 ± 6.1 Gt/year falls on the GrIS, 11.4 ± 1.4 Gt/year on the GIC, and 71.4 ± 9.0 Gt/year on the tundra. The downscaled 1 km product better resolves especially the relatively small GIC, more than doubling (+124%) their rainfall compared to the 5.5 km product. The relatively warm southern regions of Greenland have the highest rainfall amounts, with annual values locally exceeding 1,000 mm. We confirm a significant positive trend in Greenland rainfall (>40 mm/decade), notably in the northwest and mainly due to an increase in rainfall fraction (>3.5%/decade) during July and August. For the whole of Greenland, during 1991–2020 the seasonal rainfall peak has shifted from July to August, with significant increases in September, which receives more rain than June. An analysis of rainfall fraction and near-surface temperature shows that local warming rates are a good predictor of recent rainfall changes.

1. Introduction

Global warming impacts the climate of Greenland, including the Greenland Ice Sheet (GrIS), its peripheral glaciers and ice caps (GIC), and the surrounding ice-free tundra (Bintanja & Selten, 2014; Mernild et al., 2015; Shepherd & Wingham, 2007; The IMBIE team, 2020). Arctic amplification causes excess warming over Greenland (Zhang et al., 2022), and precipitation falls as rain rather than snow ever more frequently (Dou et al., 2019; Huai et al., 2021; Serreze et al., 2009). For strong climate warming scenarios, rainfall is even expected to become the dominant form of Arctic precipitation (Bintanja & Andry, 2017). Screen and Simmonds (2012) showed that a decrease of snowfall in Greenland is mainly caused by the change of precipitation phase (snow to rain) during 1989–2009, while total precipitation remained largely constant. Dou et al. (2019) found that the increase of liquid precipitation during the melting season is a key factor in the melting of Arctic sea ice. Detailed knowledge of the processes behind snowfall to rainfall changes will also contribute to more accurate assessments of the impacts on hydrology/runoff, permafrost thawing, ecosystems, sea ice retreat, and glacier melt (Bintanja, 2018) and linked social-ecological systems (McCrystall et al., 2021).

Because snowfall to rainfall depends on so many processes, such as poleward moisture transport (Hao et al., 2019; Woods et al., 2013), jet stream dynamics (Wang et al., 2019), tropospheric warming (Wang et al., 2019), surface evaporation (Bengtsson et al., 2011; Vihma et al., 2016), and cloud formation processes (Noël et al., 2019), rainfall remains a relatively poorly known factor in the climate of Greenland, including the sensitivity of the mass balance of the GrIS and GIC to climate change (Doyle et al., 2015). Increases in liquid water supply may accelerate ice flow through basal lubrication (Shannon et al., 2013; Zwally et al., 2002), accelerating mass loss (Hanna et al., 2008; Oltmanns et al., 2019; Pan et al., 2021; Shepherd et al., 2020). For instance, Doyle et al. (2015) reported widespread ice flow acceleration that extended 140 km into the GrIS interior, associated with enhanced liquid water availability from melt and rainfall. Noël et al. (2017) discuss the implications of the loss of GIC refreezing capacity through saturation of the firn layer by increased meltwater and rain. Little is known about total rainfall amounts over the Greenland tundra, in spite of most rain observations being conducted there (Cappelen, 2020; Yang et al., 1999).

In the absence of a dense network of rainfall observations and robust satellite products, regional climate models can be used to provide spatially continuous rainfall fields, provided they are critically evaluated using existing observations, including schemes to determine the phase of the precipitation (Cappelen, 2020; Steffen & Box, 2001; Yang et al., 1999). Recently, Niwano et al. (2021) used the polar nonhydrostatic regional climate model NHM-SMAP at 5 km resolution to evaluate GrIS rainfall, its extremes and trends during 1980–2019. Huai et al. (2021) used precipitation observations and seven precipitation phase identification schemes to evaluate the representation of rainfall in the regional atmospheric climate model version 2 (RACMO2.3p2) at 5.5 km resolution. Both studies found generally good agreement with each other and observations.

However, challenges still remain related to the scarcity of rainfall observations on the ice-covered parts of the island, that is, the GrIS and GIC (Cappelen, 2020; Steffen & Box, 2001; Yang et al., 1999). Moreover, even at ~5 km resolution, regional climate models poorly resolve coastal topographic features and low-lying, narrow glacier tongues and small ice caps, which further hampers the interpretation of high rainfall events in the context of regional climate change (Lenaerts et al., 2020; Tedesco et al., 2016). As a first-order correction, Huai et al. (2021) applied a simple elevation dependency to the rainfall fraction to account for the complex terrain near some of the observational sites, which showed sensitive results at some locations with pronounced topography, further highlighting the importance of improved horizontal resolution. This study builds on the 5.5 km RACMO2.3p2 rainfall evaluation results of Huai et al. (2021), by further statistically downscaling the model output to 1 km to better resolve the marginal outlet glaciers of the GrIS and topographic features on the Greenland tundra, including the GIC, which are disconnected from the main ice sheet. Methods are presented in Section 2, the results for rainfall on GrIS, GIC, and tundra are discussed in Section 3, followed by a discussion in Section 4, and conclusions in Section 5.

2. Data and Methods

2.1. Regional Climate Model

We use output of the latest version of the RACMO2.3p2, which is developed and maintained at the Royal Netherlands Meteorological Institute (KNMI) (Van Meijgaard et al., 2008). The polar version was developed by the Institute for Marine and Atmospheric Research (IMAU), Utrecht University, to specifically simulate the surface mass balance over the polar ice sheets (Noël et al., 2018). Especially relevant for this study is that RACMO2.3p2 includes, among other improvements, a new cloud scheme allowing for ice super saturation: the cloud water-to-snowfall conversion coefficient remains constant for liquid (>0°C) and mixed phase clouds (−23°C–0°C), whereas it decreases with temperature for ice clouds (<−23°C), which results in improved relative contributions of rainfall and snowfall to the total precipitation flux (Noël et al., 2015; Van Wessem et al., 2014). RACMO2.3p2 here is an extension of the data set published in Noël et al. (2019), which is forced at the lateral and upper boundaries by atmospheric reanalyzes developed by European Centre for Medium Range Weather Forecasts (ECMWF) including ERA-40 (1958–1978), ERA-Interim (1979–1989), and ERA5 (1990–2020) (Noël et al., 2019).

2.2. Downscaling Procedure

At the native resolution of 5.5 km, RACMO2.3p2 realistically captures monthly observed rainfall in Greenland (Huai et al., 2021), but in the same study it was concluded that further statistical downscaling of the rainfall fields to 1 km resolution was desirable, as was previously done with other surface mass balance components (Noël et al., 2016). The main reason is that many of the marginal glaciological features, such as narrow outlet glaciers and floating ice tongues, are typically not well resolved at 5.5 km.

Although total precipitation and snowfall negatively correlate with elevation over most of the ice sheet, the correlation is small and heterogeneous for daily totals at the margins (Noël et al., 2016, 2018). In contrast, daily snowfall fraction has a strong spatial correlation with elevation almost everywhere. Therefore, the 5.5 km daily precipitation totals are simply bilinearly interpolated onto the 1 km grid (P). Next, the 5.5 km daily snowfall fraction is statistically downscaled to the 1 km grid (S_{frac}), the downscaling algorithm corrects the snowfall fraction using the local regression to elevation and each grid using eight adjacent pixels (Noël et al., 2016). Then the 1 km daily snowfall fraction combined with P to obtain the daily, 1 km snowfall totals (S) and rainfall totals (R):
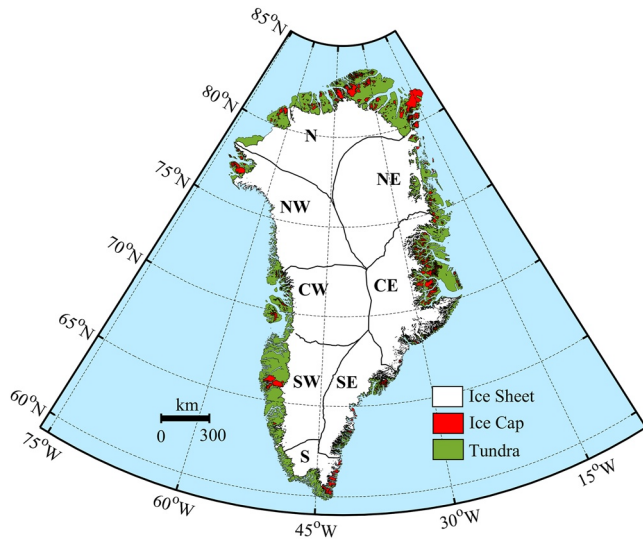
$$S = P * S_{frac} \tag{1}$$

Figure 1. The three masks representing the Greenland ice sheet (GrIS, white), peripheral glaciers and ice caps (GIC, red), and ice-free tundra (green), and eight climatological regions used in this study.

$$R = P * (1 - S_{frac}) \qquad (2)$$

In this study, we also use statistically downscaled near-surface temperature (T_{2m}) from RACMO2.3p2, again using elevation dependency.

In the following, we define rainfall fraction as the ratio of rainfall and total precipitation cumulated over a certain period (Huai et al., 2021) that will each time be clearly defined. We distinguish rainfall changes due to increased precipitation (the "amount" effect) from changes caused by an increased rainfall fraction (the "rainfall fraction" effect). The "amount effect" is first quantified by assuming the rainfall fraction to remain unchanged, and then the "rainfall fraction" effect is the total increased rainfall minus the "amount" effect.

In the analysis, we distinguish three surface masks (Figure 1): the contiguous inland ice sheet (GrIS), GIC, and the ice-free tundra (Figure 1), where we follow the definitions of Rastner et al. (2012). The eight sectors we refer to when discussing results (N, NE, CE, SE, S, SW, CW, and NW, see Figure 1) are climatologically distinct with respect to precipitation, with precipitation in, for example, the north and northeast dominated by changes in the sea-ice cover (Zwally & Giovinetto, 2001), in the southeast by the Icelandic Low, and in southwest Greenland by cyclogenesis in the Labrador Sea (Hanna et al., 2006).

2.3. Digital Elevation Models (DEM)

A 1-km ice mask and DEM are obtained by averaging the original 90 m Greenland Ice Mapping Project (GIMP, Howat et al., 2014) grid cells in each 1 km pixel covering Greenland (Noël et al., 2016). Integrated over the GIC and tundra region, the area of 81,869 km^2 (GIC) and 360,690 km^2 (tundra) for the 1 km grid represents a 5.4% and 1.4% increase relative to the 5.5 km mask. Figure 2a shows the resulting three masks color-coded at 1 km resolution, and Figures 2b–2e show two examples of regional topographies in west and southeast Greenland, resolved at 1 km (b and d) and 5.5 km (c and e) products. As can be seen, the topography at 1 km resolution better resolves small scale landforms, which in Greenland often include small ice caps, outlet glaciers, and glacier tongues (orange shading in Figure 2a). The downscaling therefore leads to a significant change in rainfall fraction over these small ice bodies, which are elaborated upon in Section 3.1.

2.4. Evaluation of the 1 km Rainfall Product

We processed rain gauge observations operated by the Danish Meteorological Institute (DMI) following Huai et al. (2021), that is, applying undercatch corrections and seven precipitation phase identification schemes. Figure S1 in Supporting Information S1 shows higher correlation and lower RMSE for some stations in the 1 km rain product.

3. Results

3.1. Long-Term (1958–2020) Average Rainfall

Table 1 lists the long-term (1958–2020) average annual precipitation, rainfall, snowfall, and associated rainfall fraction of the RACMO2.3p2 1 and 5.5 km products integrated over GrIS, GIC, tundra, and entire Greenland, and their respective surface areas. Here, we focus on the differences between the original and downscaled product. Because it has been bilinearly interpolated only and not statistically downscaled, total precipitation should in principle not change; the small increase (+1.9%) in total precipitation between the two products arises from the different integration areas (+1.2%). The most significant changes are found for rainfall and rainfall fraction. Compared to the 5.5 km product, the largest relative rainfall increase occurs for the GIC (+6.3 Gt/year, or +124%). Over the GrIS and tundra regions, the absolute annual rainfall increases compared to the 5.5 km products are also significant: +12.4 Gt/year (+45%) and +16.6 Gt/year (+30%). For all three masks, these increases
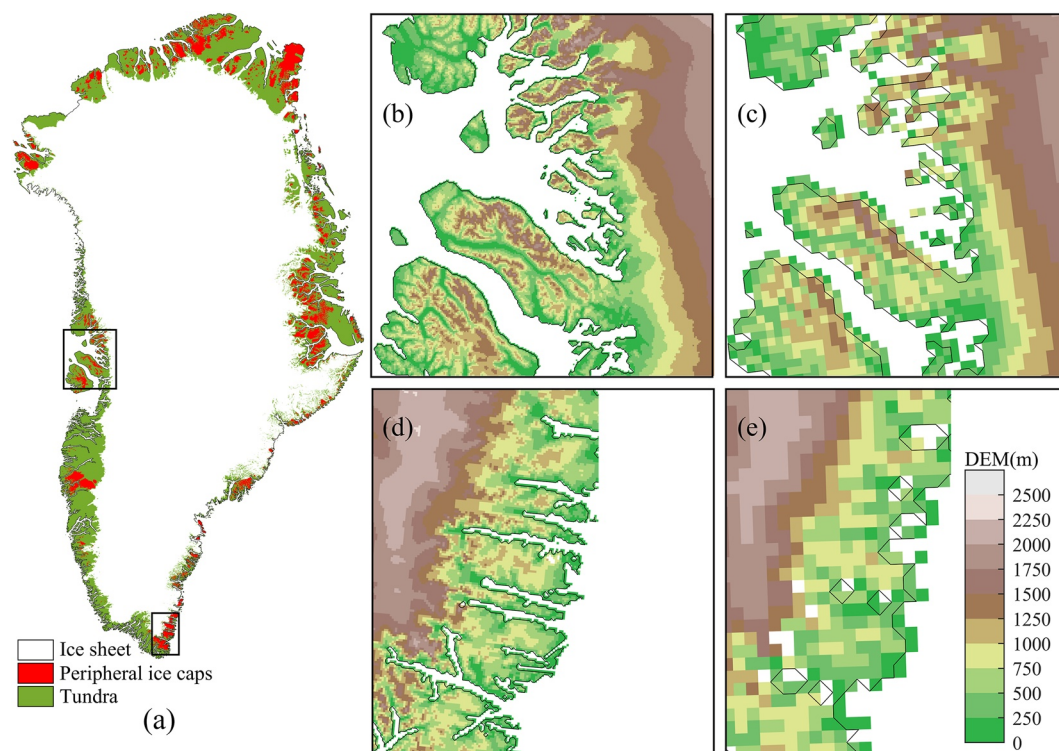
Figure 2. Masks of tundra, glaciers and ice caps, and Greenland ice sheet at 1 km resolution (a) and regional (CW and SE) comparisons of topography in RACMO2.3 at 5.5 km (c and e) with Greenland Ice Mapping Project at 1 km (b and d).

are significantly larger than the increases in those of surface area, which are +0.9% (GrIS), +5.4% (GIC), and +1.4% (tundra). In the 1 km product, the average annual rainfall in Greenland during 1958–2020 is 111.4 Gt/year: 28.6 Gt/year on the GrIS, 11.4 Gt/year on the GIC, and 71.4 Gt/year on the tundra with rainfall fractions of 4.2%, 17.6%, and 31%, respectively.

In a previous model version (RACMO2.1) run at 11 km resolution over Greenland and for the period 1958–2007, Ettema et al. (2009) found higher values for the combined GrIS and GIC (44.6 Gt/year, rainfall fraction 6%). Our results for the same period (1958–2007) for GrIS and GIC rainfall are 40.1 Gt/year (1 km) and 27.3 Gt/year (5.5 km), with rainfall fractions of 5.2% and 3.6%, respectively. For RACMO2.3p1 at 11 km, Van den Broeke et al. (2016) reported a 1991–2005 annual rainfall (fraction) over the GrIS of 28 Gt/year (3.9%). For the same period and mask, here we find 41.3 Gt/year (1 km) and 30.8 Gt/year (5.5 km) of rainfall, with rainfall fractions of 5.3% and 3.9%, respectively. Two studies with different regional climate models (MAR, Fettweis et al., 2013, and NHM-SMAP, Niwano et al., 2021) reported annual rainfall of 25 and 28 Gt/year for the period 1980–1999, respectively. For the same period (1980–1999) our results show 39.7 Gt/year (1 km) and 27.5 Gt/year (5.5 km).

From these comparisons we conclude that the native 5.5 km RACMO2.3p2 rainfall product agrees well with recent previous estimates from models with similar physics and resolution. Therefore, the rainfall increase resulting from statistical downscaling to 1 km resolution represents a significant increase compared to previous work.

To look at these differences in more detail, Figure 3 shows two examples of GIC regions where the 1 km product shows significant increases in rain on

Table 1

Long-Term (1958–2020) Multiyear Average Annual Total Precipitation (P), Rainfall (R), Snowfall (S, All Gt), Rainfall Fraction (R_{frac},%), and Area (km^2) for RACMO2.3p2 1 and 5.5 km Products, Integrated Over GrIS, Glaciers and Ice Caps, Tundra, and Entire Greenland

RACMO2.3p2	GrIS	GIC	Tundra	Greenland
P 5.5 km (Gt)	688.7	61.6	224.9	975.1
R 5.5 km (Gt)	22.6	5.1	54.8	82.4
S 5.5 km (Gt)	666.3	56.5	170.1	892.7
R_{frac} 5.5 km (%)	3.3	8.3	24.4	8.5
Area 5.5 km (km^2)	1,684,864	77,652	355,770	2,118,287
P 1 km (Gt)	699.1	64.6	230.0	993.3
R 1 km (Gt)	28.6	11.4	71.4	111.4
S 1 km (Gt)	670.1	53.2	158.6	881.9
R_{frac} 1 km (%)	4.1	17.6	31.0	11.2
Area 1 km (km^2)	1,700,836	81,869	360,690	2,143,395

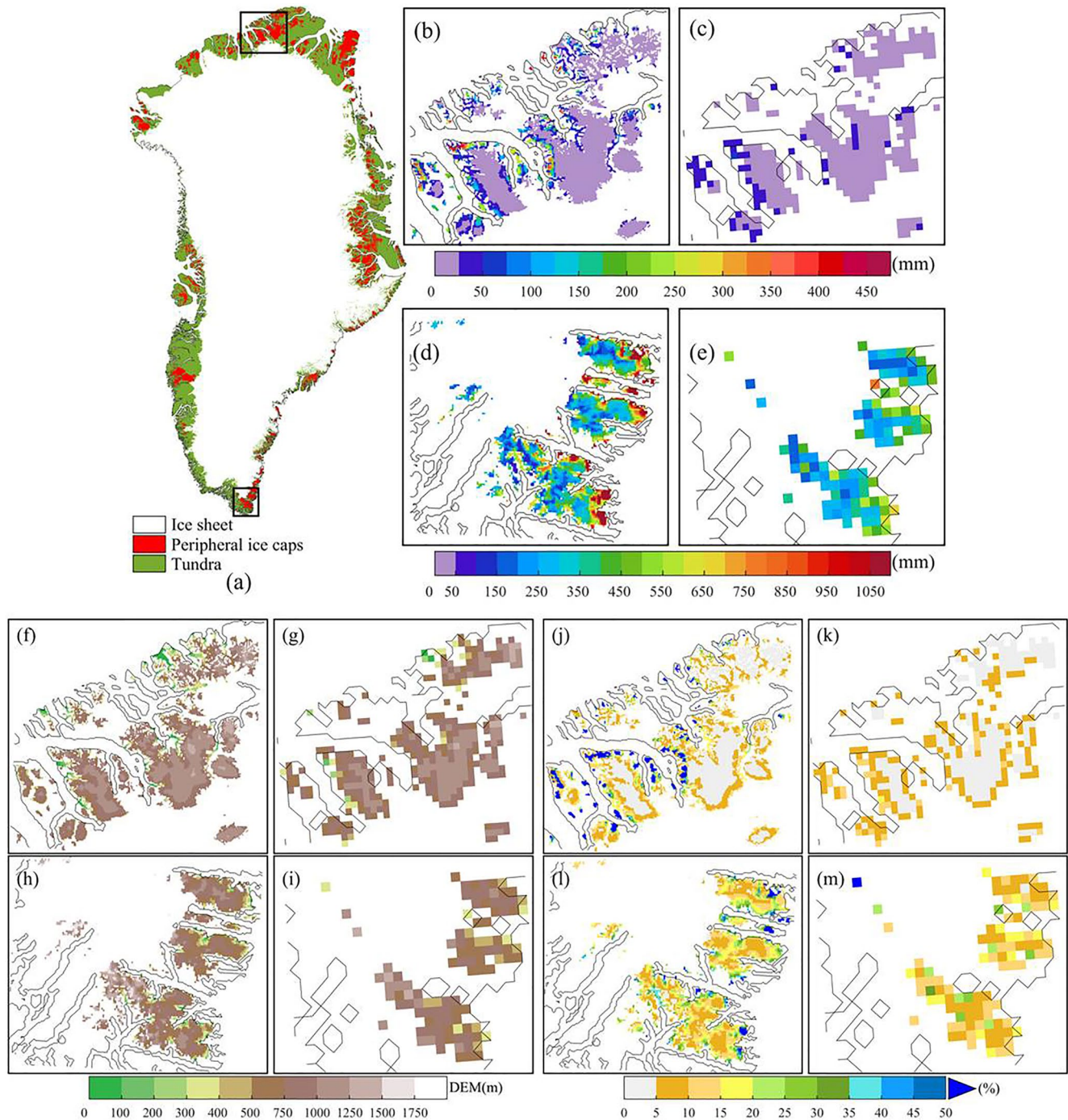*Note.* Rainfall fraction based on cumulative totals for the full period.

Figure 3. RACMO2.3 average annual rainfall (mm/year) during 1958–2020 for selected northern glaciers and ice caps (GIC) at 1 km (b) and 5.5 km (c); selected southern GIC at 1 km (d) and 5.5 km (e); topography (f–i; m); average annual rainfall fraction (j–m; %).

ice compared to the 5.5 km product. For the selected northern GIC (Figures 3b and 3c), the multiyear annual rainfall differences between the two products is 0.25 Gt (+174%). At 5.5 km resolution, in this cold climate almost no rainfall (<50 mm/year) is simulated (Figure 3c). In contrast, the 1 km product predicts high rainfall values on the wet, seaward facing slopes (>450 mm/year), on low-lying glacier margins (Figure 3b). For the selected southern GIC (Figures 3d and 3e), the climate is milder and significant rainfall is also simulated in the 5.5 km product. Still, the increase in the 1 km product is considerable at 0.98 Gt/year (+64%), with absolute differences up to 500 mm/year over wet, seaward facing margins. In the presence of the Icelandic Low, especially the seaward
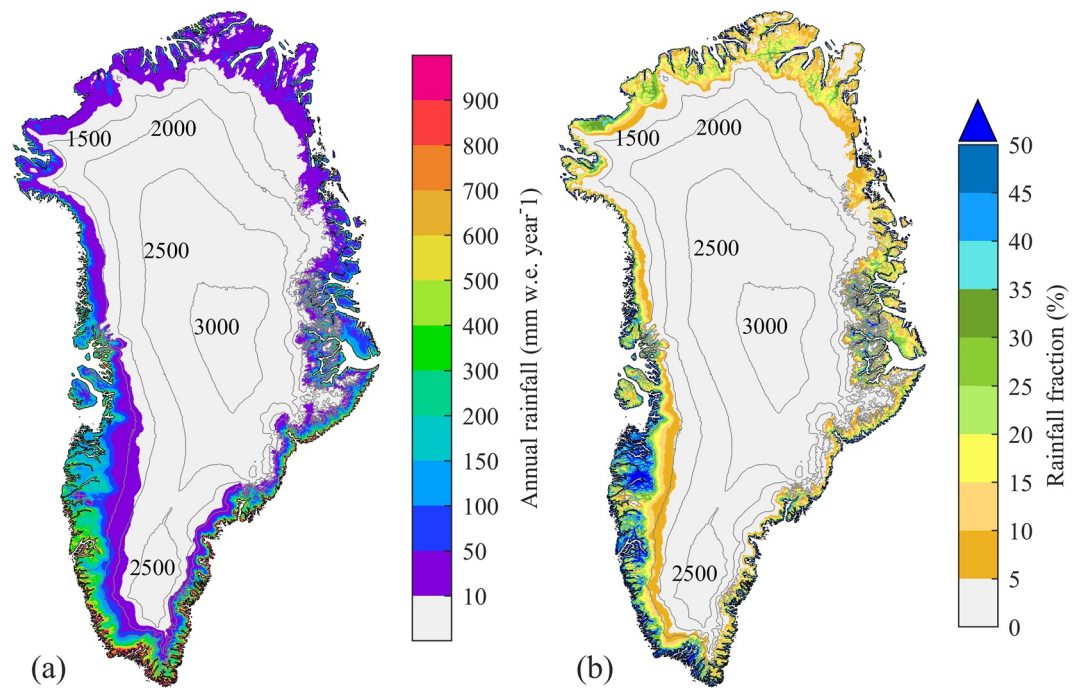
Figure 4. (a) Long-term (1958–2020) average annual rainfall (mm/year) and (b) rainfall fraction (%), based on 1958–2020 cumulative totals at 1 km resolution. The gray lines represent 500 m elevation contours.

facing slopes of the southeast GrIS, GIC, and tundra receive high amounts of topographically forced precipitation (Mernild et al., 2015). In combination with relatively mild conditions, these results in rainfall rates in the 1 km product that locally exceed 1,000 mm/year, the highest values found in Greenland.

To explain these differences, Figures 3f–3m show the corresponding topography (for ice covered regions only) and rainfall fraction for two selected northern and southern GIC regions in the 1 and 5.5 km products. The topography at 1 km resolution reveals low-lying glaciated regions (especially <500 m asl) that are now much better resolved (Figures 3f and 3h). At 1 km resolution, rainfall is high both in absolute amount and as fraction of the total precipitation, in multiple regions exceeding 50%. The multiyear annual rainfall fraction for the selected southern GIC < 500 m a.s.l. (above sea level) increases by 7.1% and in the northern GIC < 500 m a.s.l. by 6% (Figures 3b and 3d). We conclude that the improved representation of low-lying, warmer glaciated areas explains the enhanced rainfall in the 1 km product.

To compare modeled to observed rainfall, Huai et al. (2021) applied an elevation correction to the modeled snowfall fraction in RACMO2.3p2 to account for the complex terrain at some observational sites not well resolved at 5.5 km resolution. After doing so, they showed that even at 5.5 km resolution, RACMO2.3p2 simulates rainfall at the observational sites with reasonable accuracy. When applying such corrections to the full gridded data, the above examples show that regionally, away from the observational sites, the representation of rainfall in Greenland in the 1 km product can differ significantly from the 5.5 km product, making it a useful tool to further analyze spatial and temporal variability of rainfall in Greenland. Figure 4 shows the long-term (1958–2020) average annual rainfall for the 1 km product (mm/year, Figure 4a), and the corresponding rainfall fraction, that is, based on 1958–2020 cumulative totals (%, Figure 4b). In line with the 5.5 km product discussed in Huai et al. (2021), the extreme south and southwest of Greenland receive most rainfall, but values in the 1 km are higher, locally in excess of 1,000 mm/year. The 1 km grid cell with the highest modeled rainfall total in Greenland is situated at 42.95°W, 61.02°N in the ablation zone of one of the SE GIC at an elevation of 1,064 m a.s.l.; this location receives on average 4,925 mm of rainfall per year and has a rainfall fraction of 87%.

The model simulates regional variations in annual average rainfall over Greenland. The dominating large-scale patterns in Figure 4a show a generally decreasing rainfall amount with increasing latitude and elevation, a result of lower temperatures and the topographic effect of near-coastal mountains, but again with large regional and

local deviations. For example, the total rainfall over southwestern Greenland, with a wide tundra region, a gently sloping ice sheet margin and higher summer temperatures, generally exceeds the total rainfall at the same latitude in the southeast, where the ice sheet is steeper with only a narrow strip of ice-free tundra.

The long-term (1958–2020) rainfall fraction in Figure 4b is obtained by dividing the full-period cumulative totals of rain and total precipitation. Even in the far northwest and north, rainfall fractions as high as 35% are found, mainly over the flat coastal tundra away from the coast. The highest rainfall fractions in Greenland, in excess of 60%, are found over the southwestern tundra, also away from the coast. This agrees with previous estimates of Box et al. (2006), who used the Polar MM5 regional climate model and also simulated rainfall fractions up to 60% along the extreme southwest margin. High rainfall fractions of up to 40% are also modeled over the GrIS, notably the lowest parts of the marginal ice sheet in southwest Greenland.

3.2. Interannual Variability and Trends in Rainfall

Figure 5 illustrates 1958–2020 time series of annual total precipitation, snowfall, rainfall, and rainfall fraction (based on annual totals) for the 1 km (red) and 5.5 km (blue) products and integrated over the GrIS (first column), GIC (second column), and the tundra regions (third column). The bold numbers represent the standard deviations in the time series. Table 2 lists the trends with uncertainties based on a linear regression (dashed lines in Figure 5). Total precipitation and snowfall show modest relative differences (<10%) between the two products. The trends in total precipitation are positive for all three masks (Table 2) but the significance levels are low ($1 - p$ values for GrIS: 0.55, GIC: 0.40, and tundra: 0.54), owing to the large natural variability of the signal. An interesting contrast appears in the trends of snowfall and rainfall. Over the GrIS, the increase in snowfall explains 72% of the increase in total precipitation both for the 1 and 5.5 km products. This differs from the GIC and tundra, where snowfall trends are essentially zero and the increase in total precipitation is fully driven by increased rainfall. Both products show significantly positive rainfall trends for all three masks (all pass the significance test at the 95% confidence level); however, the 1 km product has more rainfall in absolute sense, while the 5.5 km products show stronger rainfall trends, that is, the rainfall fraction increases more rapidly in the 5.5 km product than in the 1 km product. This is likely a hypsometry driven result, as the higher, flatter regions that experience rainfall are also better represented by the increasing rate in the 5.5 km product.

For the whole of Greenland and for the full period (1958–2020), rainfall in the 1 and 5.5 km products increases by 2.64 and 3.66 Gt/decade, with high confidence ($1 - p$) values of 0.99 and >0.99, respectively. Most significant is the rainfall increase over GIC (0.3 and 0.3 Gt/decade for 1 and 5.5 km, with confidence levels ($1 - p$) values of >0.99 and >0.99), while the tundra region rainfall increases with 1.3 and 1.9 Gt/decade (with confidence levels ($1 - p$) values of 0.97 and >0.99). The interannual variability of rainfall is high. On the GrIS, year-to-year variations of rainfall can be extreme, for example, a 149%/136% increase from 2009 to 2010 for the 1 km/5.5 km products. For GIC, we find even higher interannual changes of 169% and 147% for the same years.

Figure 6 shows time-varying trends (Gadedjisso et al., 2021; Hanna et al., 2021) of rainfall (fraction) for the three masks. The period 1990–2010 experienced the most significant rainfall increase for the GrIS (12 mm/decade), GIC (2–3 mm/decade), and tundra (12–15 mm/decade), all significant at the 95% level. From 1990 onwards, the increase in rainfall fraction for the majority of the periods is also significant. We conclude that the increase in rainfall after 1990 is mainly caused by a significant increase in the rainfall fraction, which applies to GrIS, GIC, and the tundra regions. This abrupt change starting in 1990 is also found in time series of GrIS surface mass balance, which has been significantly decreasing since the 1990s (Noël et al., 2020). Hanna et al. (2008) attributed this to significantly increased Greenland summer warmth and associated stronger GrIS melt and runoff. Noël et al. (2019) reported a similar jump in GrIS integrated meltwater runoff in 1990. An estimated 3.8%–4.0% (Hanna et al., 2008) of this recent runoff increase can be ascribed to increased rainfall (which runs off immediately when it falls on impermeable ice) rather than only to increased melt. In contrast, Figure 6 shows that an earlier period with a significant rainfall increase (1965–1978) is evidently caused by an increase in total precipitation ("amount effect") because it did not correspond to a concurrent significant increase in the rainfall fraction. Several other episodes with decreases in rainfall (fraction) are not found to be significant.

The time-varying trends are far from spatially uniform. Figure S2 in Supporting Information S1 shows maps of the annual rainfall anomalies for the period 1958–1975 and 1991–2020, relative to 1958–2020. The mainly dry anomalies during 1958–1975 occurred in almost all of the coastal regions in Greenland, with the highest
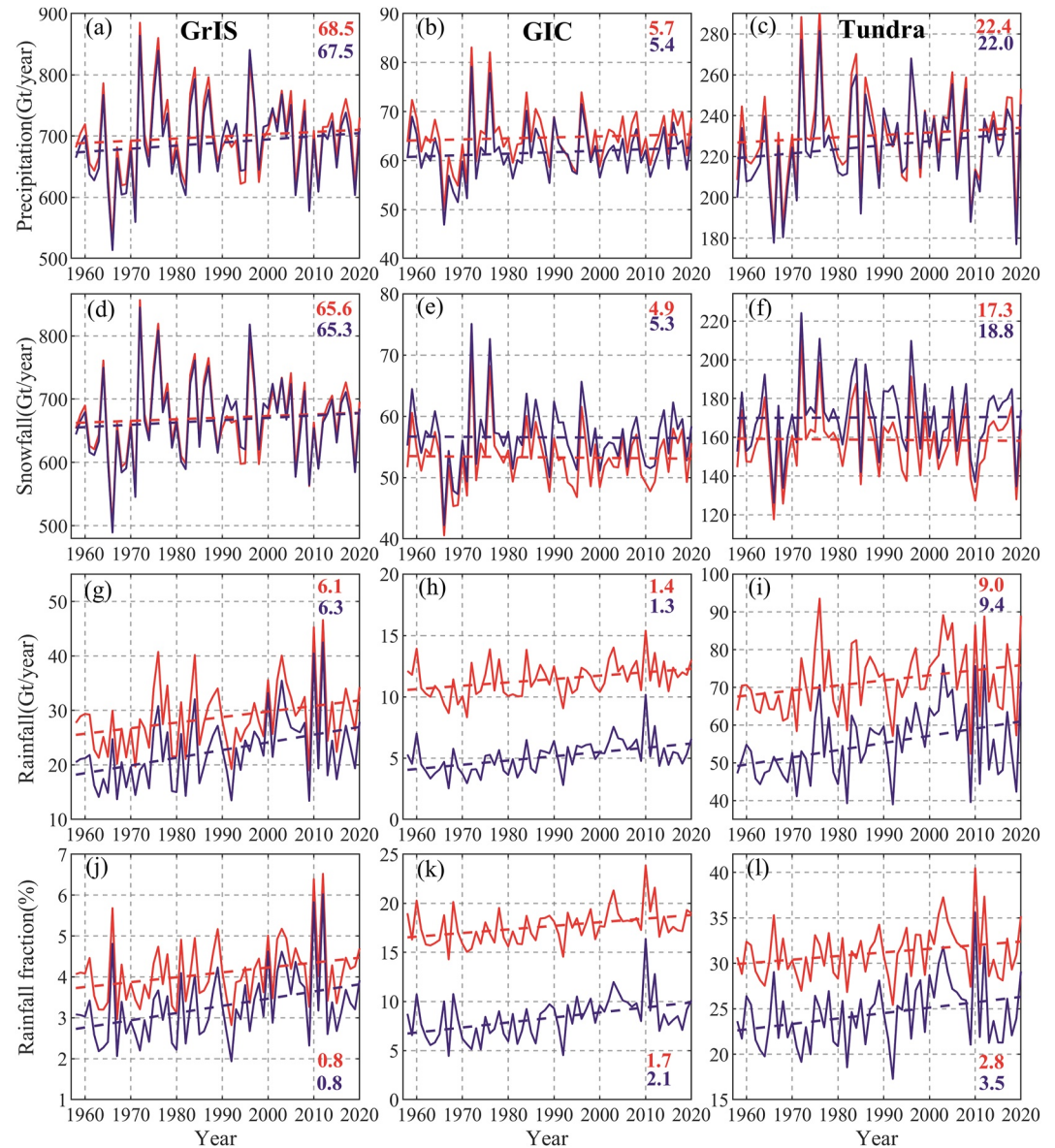
Figure 5. Time series of annual total precipitation (first row), snowfall (second row), rainfall (third row, all in Gt), and rain fraction (fourth row, %, based on annual totals) integrated over Greenland ice sheet (first column), glaciers and ice caps (second column), and tundra (third column). RACMO2.3p2 1 km (red line) and 5.5 km (blue line) products. The bold numbers that represent the standard deviations and trend magnitudes (dashed lines) can be found in Table 2.

magnitudes along the southwestern margin, up to −116 mm/year (−19%). The mainly wet rainfall anomalies during 1991–2020 occurred mainly in the northwestern and southern regions. In contrast, some regions in southwest Greenland exhibited less rainfall during 1990–2020.

3.3. Rainfall Seasonality

Figure 7 shows average (1958–2020) seasonal rainfall totals and rainfall fraction for the 1 km RACMO2.3p2 rainfall product. In spring and winter (Figures 7a and 7d), only the warm and wetter south and southwestern coastal regions receive significant rainfall. In fall, rainfall in the southwest is significantly higher than in spring (Figure 7c), which could be explained in part by the lower sea ice cover to the west of Greenland (Kopec et al., 2016). Seasonal maximum rainfall occurs in summer in the southwest (Figure 7b). During summer, the entire coast of Greenland is sea ice free promoting evaporation and precipitation, which in the warmer regions

Table 2
Linear Regression Parameters: Trend in Gt per Decade and Confidence Level $(1 - p)$

Region	Variables	Trend (Gt/decade)		$1 - p$	
		1 km	5.5 km	1 km	5.5 km
GrIS	Precipitation	3.6	5.1	0.55	0.72
	Snowfall	2.6	3.7	0.42	0.54
	Rainfall	**1.0**	**1.4**	0.99	1.00
	Rainfall fraction	**0.1**	**0.2**	0.98	1.00
GIC	Precipitation	0.2	0.3	0.40	0.58
	Snowfall	−0.1	0.0	0.16	0.09
	Rainfall	**0.3**	**0.3**	1.00	1.00
	Rainfall fraction	**0.4**	**0.5**	1.00	1.00
Tundra	Precipitation	1.2	2.0	0.54	0.81
	Snowfall	−0.2	0.1	0.12	0.05
	Rainfall	**1.3**	**1.9**	0.97	1.00
	Rainfall fraction	**0.4**	**0.6**	0.96	0.99

Note. Trends in bold represent values that pass the significance test at the 95% confidence level.

falls mainly as rain. Summer rainfall ranges from 10 to 200 mm in the north to 50–400 mm in the southwest. In west Greenland, significant summer rainfall extends far (up to 200 km) onto the inland ice sheet.

The seasonal rainfall fractions (%), based on 1958–2020 totals, exhibit maximum values in summer, where most (>50%) of precipitation on the tundra falls as rain, except for the far north. Values of the rainfall fraction range from 30% to 60% on the northern to 70%–100% on the western tundra. On the lower ice sheet in west Greenland up to 40% of the precipitation falls as rain, with values up to 20% in the other parts of the GrIS. Rain fractions are higher in fall than in spring. In fall (Figure 7g), rainfall fractions of up to 50% are modeled in southwest Greenland. In winter (Figure 7h), significant rain fractions (up to 15%) are predicted only in some isolated patches in the west, east, and far south.

To study recent changes in rainfall seasonality, Figure 8a compares the average seasonal cycle of rainfall for two periods: 1958–1990 and 1991–2020. Error bars represent the standard deviation. The most remarkable result is the shift of the rainfall peak toward late summer, with rainfall on the GrIS, GIC, and tundra all showing significant increases in August and September. The average August/September tundra rainfall during 1991–2020 is 2.1/2.1 Gt (17/25%) higher than during 1958–1990. On the GrIS, these changes are 30/32% for August/September, respectively. Figure S3 in Supporting Information S1 shows the corresponding seasonal cycle of rainfall fraction for these two periods. It shows that the average August/September tundra rainfall fraction during 1991–2020 is 5.7/5.5% (10.0/15.7%) higher than during 1958–1990. On the GrIS, rainfall fraction increases by 1.6/1.1% in August/September, respectively.

Niwano et al. (2021) also reported September rainfall fraction to be increasing, by 3.4% in 40 years between 1980 and 2019, with a rainfall increase of 7.5 Gt/month for the whole ice sheet. These results support previous results that synoptic conditions favorable for rainfall drove the late-August changes across southwestern Greenland, where August is the wettest month (Doyle et al., 2015). This also conforms to Schuenemann and Cassano (2010), who reported that climate change is increasing the magnitude of precipitation events with a shift to later in the summer, especially in southwestern Greenland.

Figure 8b represents the seasonal cycle of absolute rainfall change (Gt) during 1991–2020 compared to 1958–1990 integrated over the GrIS, GIC, and tundra. August and September contribute the most to the rainfall increase. Figure 8c partitions the changes in the seasonal monthly rainfall into contributions from increased precipitation (the "amount" effect) and from increased rainfall fraction. The GrIS, GIC, and tundra regions all show increased rainfall due to increased rainfall fractions in summer (except July), as well as in September and October. In contrast, the "amount" effect is negative in June and July and even leads to reduced July rainfall in Greenland. In August and September this reverses into a positive contribution, strengthening the increase resulting from the higher rain fraction. Overall, during the main rain months, the rainfall increases over GrIS, GIC, and tundra are predominantly caused by increased rainfall fractions, that is, in June (73%, 63%, and 52%), August (65%, 81%, and 63%), and September (75%, 75%, and 64%), respectively.

To assess the spatial distribution of the changes, focusing on the months June–September, Figure 9 shows 1958–2020 trends in rainfall (mm/decade) and rainfall fraction (%/decade) for June, July, August, and September. Figure S4 in Supporting Information S1 shows the same but only for the regions which pass the 95% significance test. The positive rainfall trends are significant in the northwest for July and August, and in the southwest and southeast for September. For the northwest, the annual rainfall increase of >40 mm/decade occurred mainly during July and August. This is in agreement with Niwano et al. (2021), who also argue that the northwest sector stands out as a hotspot for rainfall increase. For August, most western coastal regions show a significant positive rainfall trend. September rainfall increases are found in the south and southwest and central east of Greenland. The monthly rainfall fraction trends (Figures 9e–9h) show similar spatial patterns, except for northwest
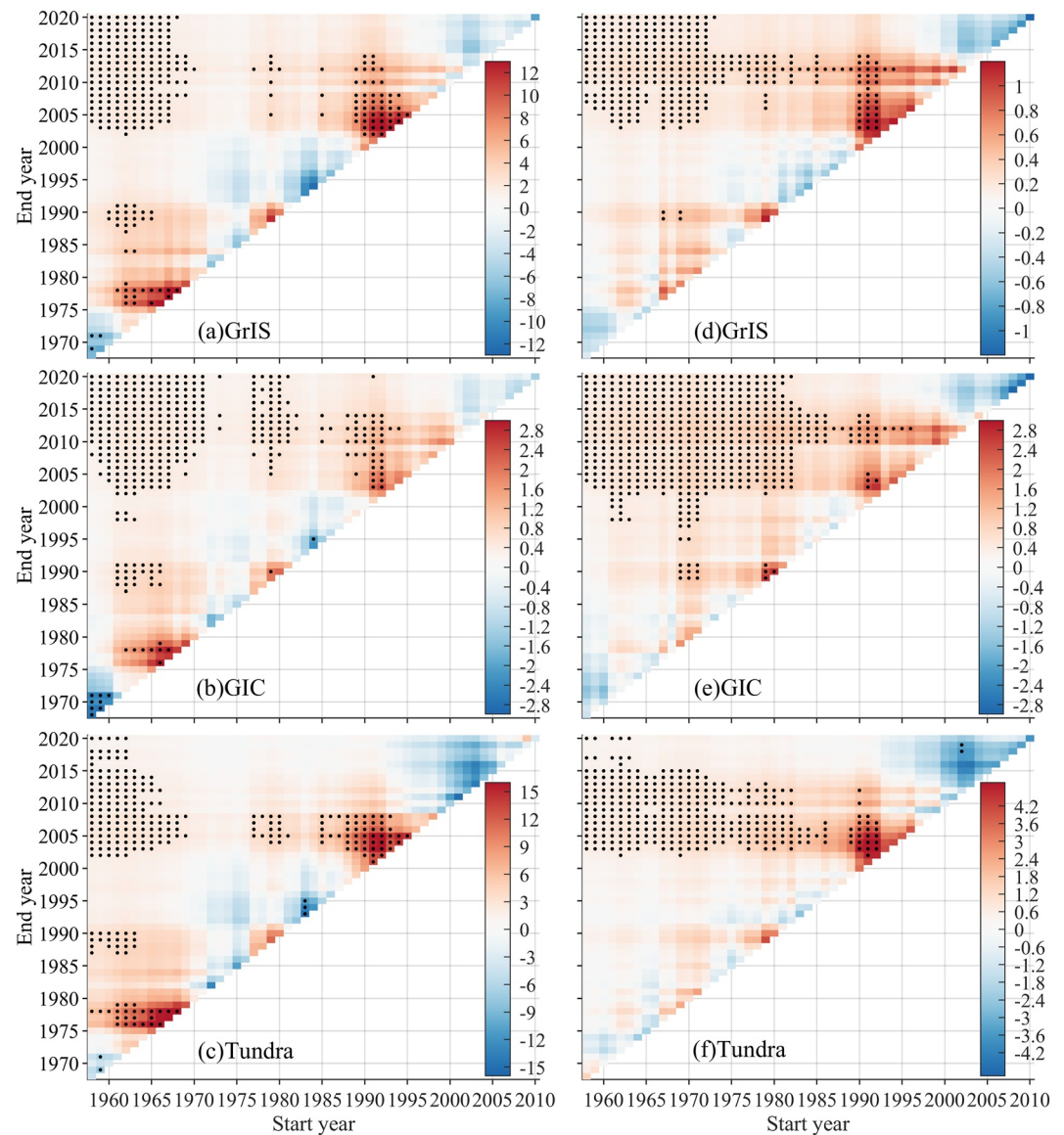
Figure 6. Time-varying trends for Greenland ice sheet (upper row), glaciers and ice caps (middle row), and tundra (lower row) of rainfall (first column; mm/decade) and rainfall fraction (second column; %/decade). Black dots represent statistically significant (at 95%) trends. Based on 1 km RACMO2.3p2 rainfall product.

Greenland in August, indicating that the amount effect (increase in total precipitation) dominated the rainfall increase in that region and month.

We find a significant rainfall decrease in southwest Greenland in July (Figure 9b), accompanied by a decrease in the rainfall fraction (Figure 9f). Lewis et al. (2019) also reported decreasing accumulation rates using snow radar and firn core data, which they attributed to shifting storm tracks related to stronger recent atmospheric summer blocking over west Greenland. The associated anticyclonic circulation anomaly over west Greenland also explains the simultaneous July increases in northwest Greenland.

4. Discussion

To better understand the underlying causes of the rainfall changes, Figure S5 in Supporting Information S1 shows the average annual total precipitation and annual rainfall increase during 1991–2020 compared to 1958–1990 (Figures S5a and S5b in Supporting Information S1), together with the contributions from increased total
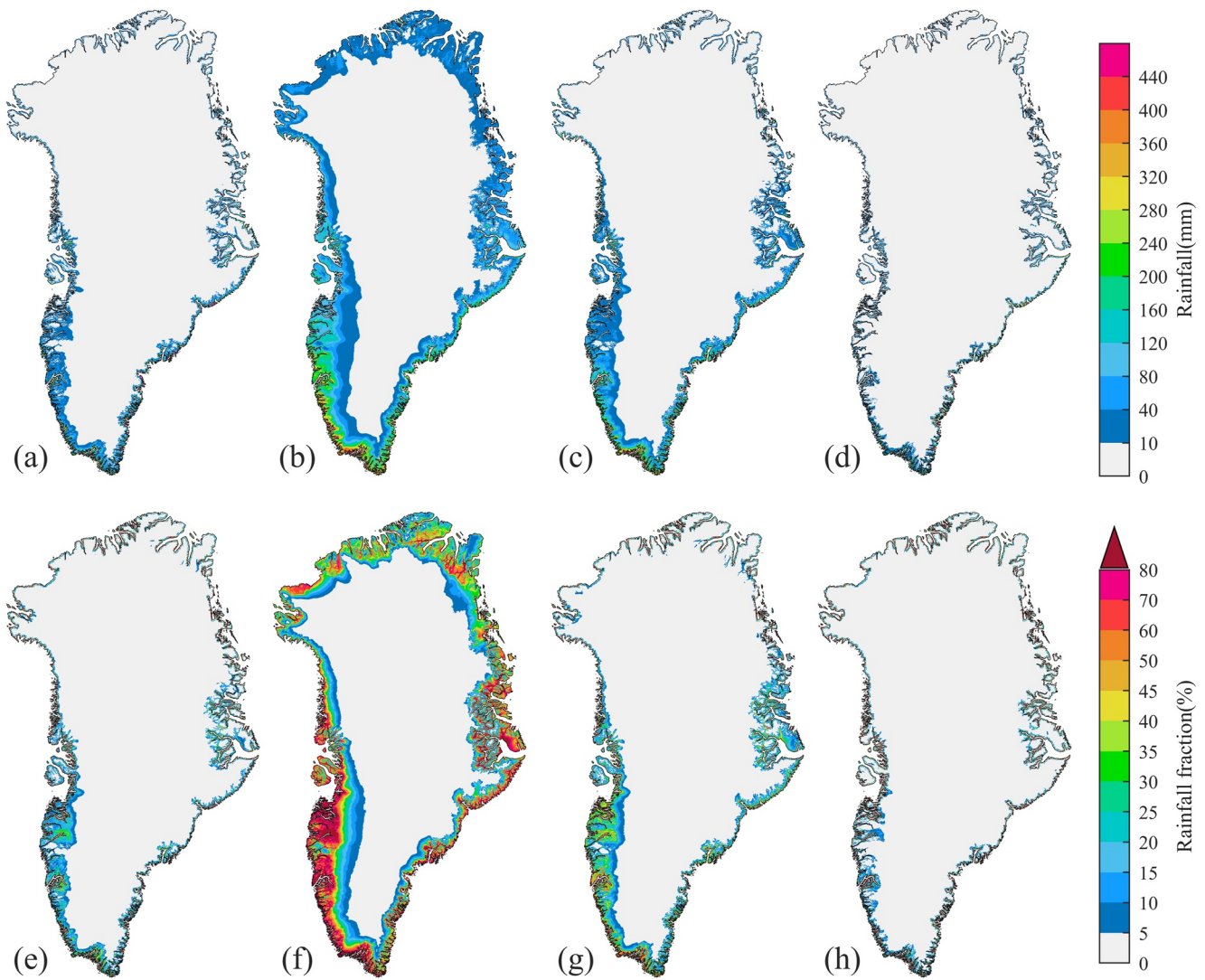
Figure 7. Average (1958–2020) seasonal rainfall (mm) for (a) spring (MAM), (b) summer (JJA), (c) fall (SON), and (d) winter (DJF) and seasonal rainfall fraction (%) for (e) MAM, (f) JJA, (g) SON, and (h) DJF.

precipitation (the "amount" effect, Figure S5c in Supporting Information S1) and by increased rainfall fraction (Figure S5d in Supporting Information S1). The "amount" effect due to a change in total precipitation shows a decrease for the southern coastal regions and an increase in the northeast. The change in rainfall fraction explains the rainfall increase along most of Greenland's coastal regions, and played a dominant role (52%~81%) in increasing rainfall in Greenland.

Figure 10 illustrates June to September rainfall changes (1991–2020 minus 1958–1990) partitioned in the contribution from the amount effect (Figures 10a–10d) and from an increased rainfall fraction (Figures 10e−10h). The contributions exhibit complex geographical patterns, with both peak values in August (Figure S4 in Supporting Information S1 and Figure 8b). Overall, compared to the "amount" effect, the contribution of a change in rainfall fraction has led to a rainfall increase in Greenland's coastal regions from June to September (up to 23 mm/month).

To further improve our understanding of the processes driving the increased rainfall fraction and its spatial patterns, we correlate rainfall fraction with near-surface temperature (T2m). We do so for summer, when the strongest dependencies and correlations are found. Figure 11a presents the summertime (JJA) rainfall fraction dependency (linear regression slope for all years in the period 1958–2020) on T2m, and Figure 11b presents the correlation coefficient. In general, the positive correlations are strongest over tundra regions in the west and north
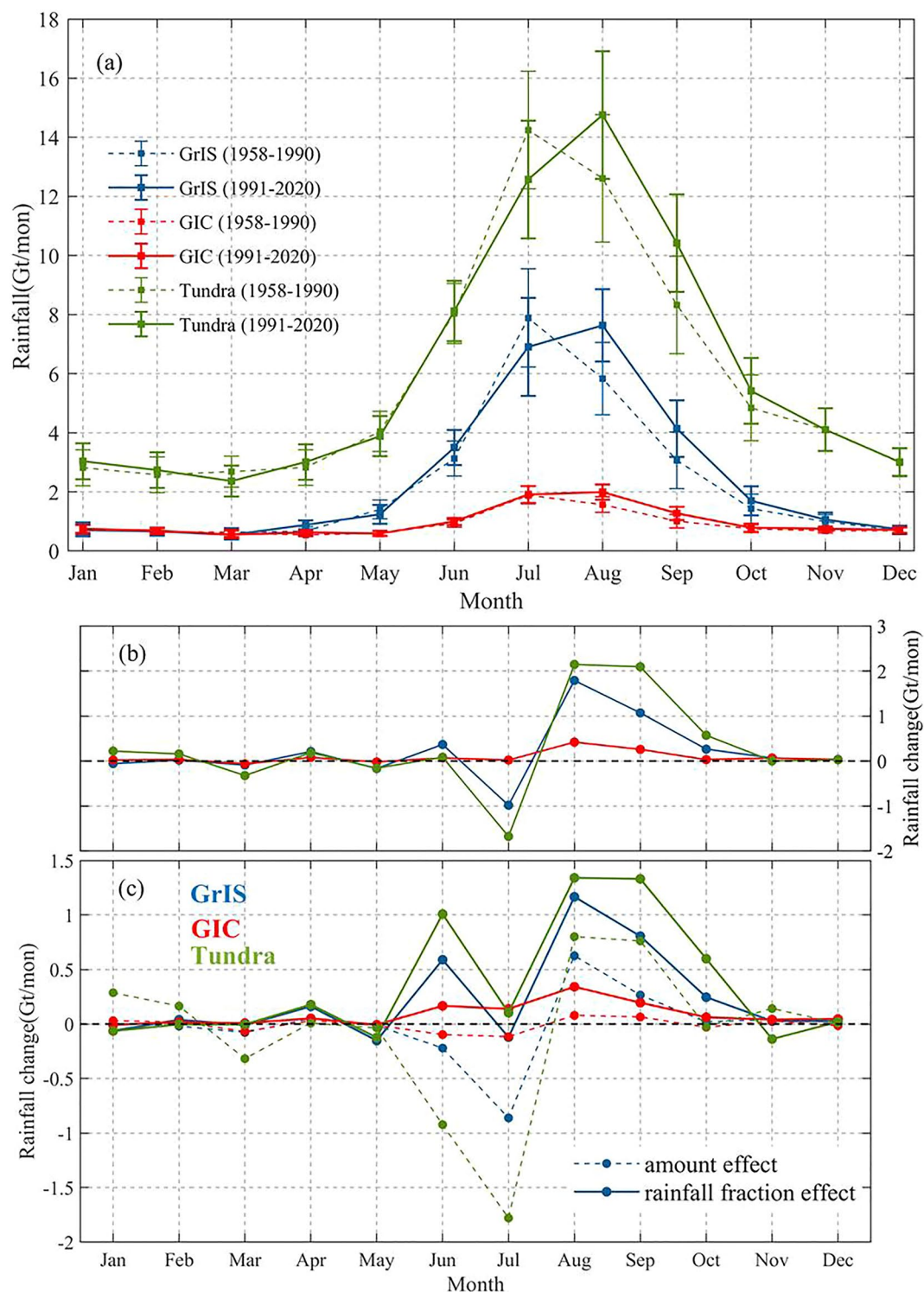
Figure 8. Seasonal cycle of rainfall for the Greenland ice sheet (blue), glaciers and ice caps (red), and tundra (green), based on monthly averages during 1958–1990 and 1991–2020. Error bars represent the standard deviation (a); seasonal cycle of rainfall change between 1958–1990 and 1991–2020 (b); partitioning of the rainfall change in a contribution from total precipitation (amount effect, dashed line) and contribution from increased rainfall fraction (solid line) (c).
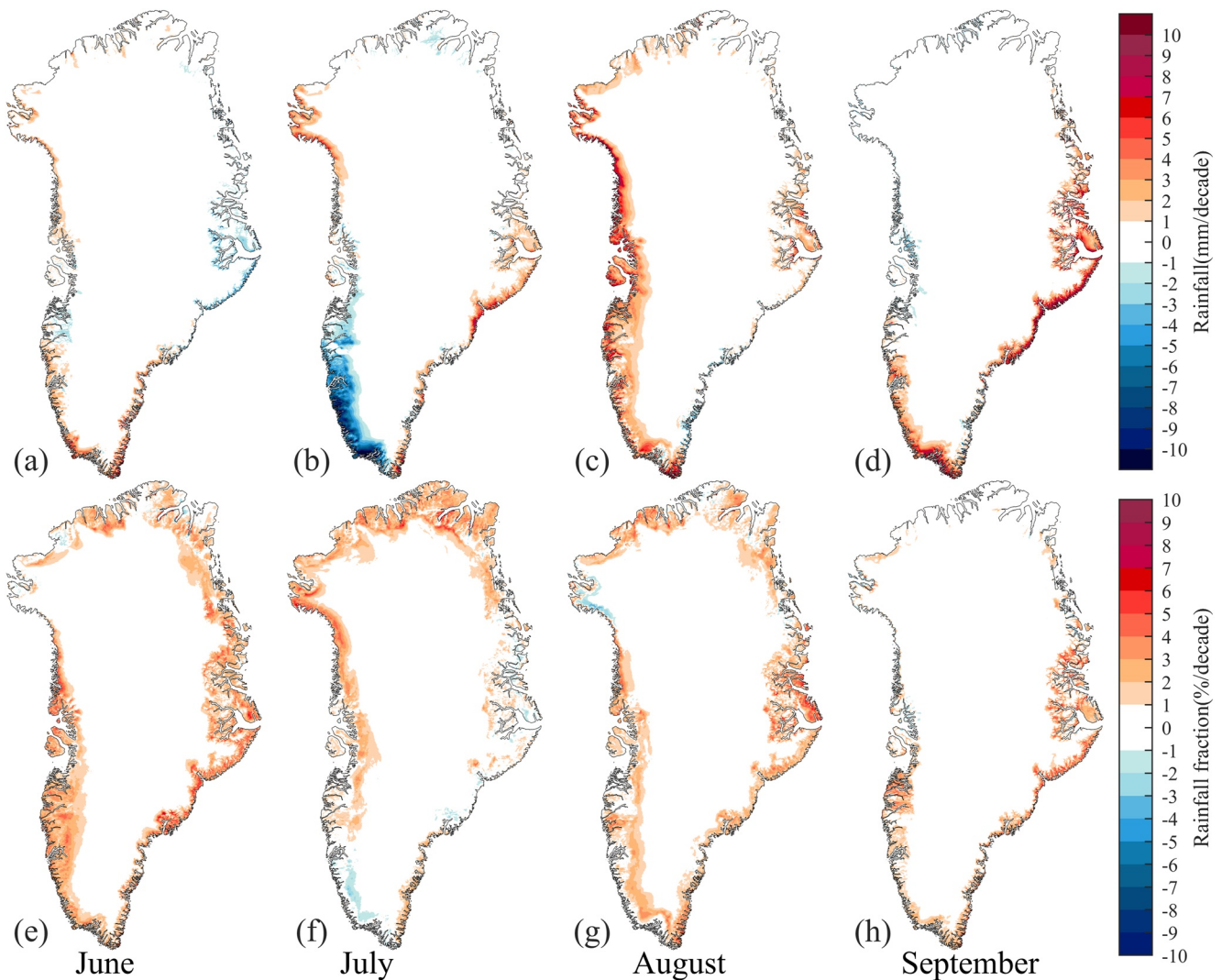
Figure 9. Trends in rainfall (mm/decade, a–d) and rainfall fraction (%/decade, e–h) for June, July, August, and September during 1958–2020 from the 1 km RACMO2.3p2 product.

and become weaker inland. This is a direct result of flattening regression curves to zero in regions where rain never occurs (Figure 11a). In Figure 11a, in addition to the temperature effect, we also see an amount effect over the slopes, where precipitation and hence rainfall is enhanced by the topography. As a result, if coastal Greenland warms by just 1°C in summer, the rainfall increase over the lower ice sheet slopes can be as large as 20%, significantly more than would be expected from thermodynamic processes alone (~7%) (Endo & Kitoh, 2014). Over the GrIS and GIC, an alternative explanation for the high sensitivity is the damping effect of the melting ice surface in summer on T2m variability.

To explain the increase in the amount of liquid precipitation, Box et al. (2006) pointed to an overall increase in temperature concentrated along the west and southeast ice sheet margins and along the topographic divide. Previous studies confirmed the conclusions that a warmer Arctic leads to increased rainfall (Bintanja, 2018; McCrystall et al., 2021) and increased poleward moisture transport (Hao et al., 2019). Our results show that increases in Greenland rainfall can be partly but not solely attributed to a local temperature increase, and that the topography relative to the large-scale circulation also plays an important role.
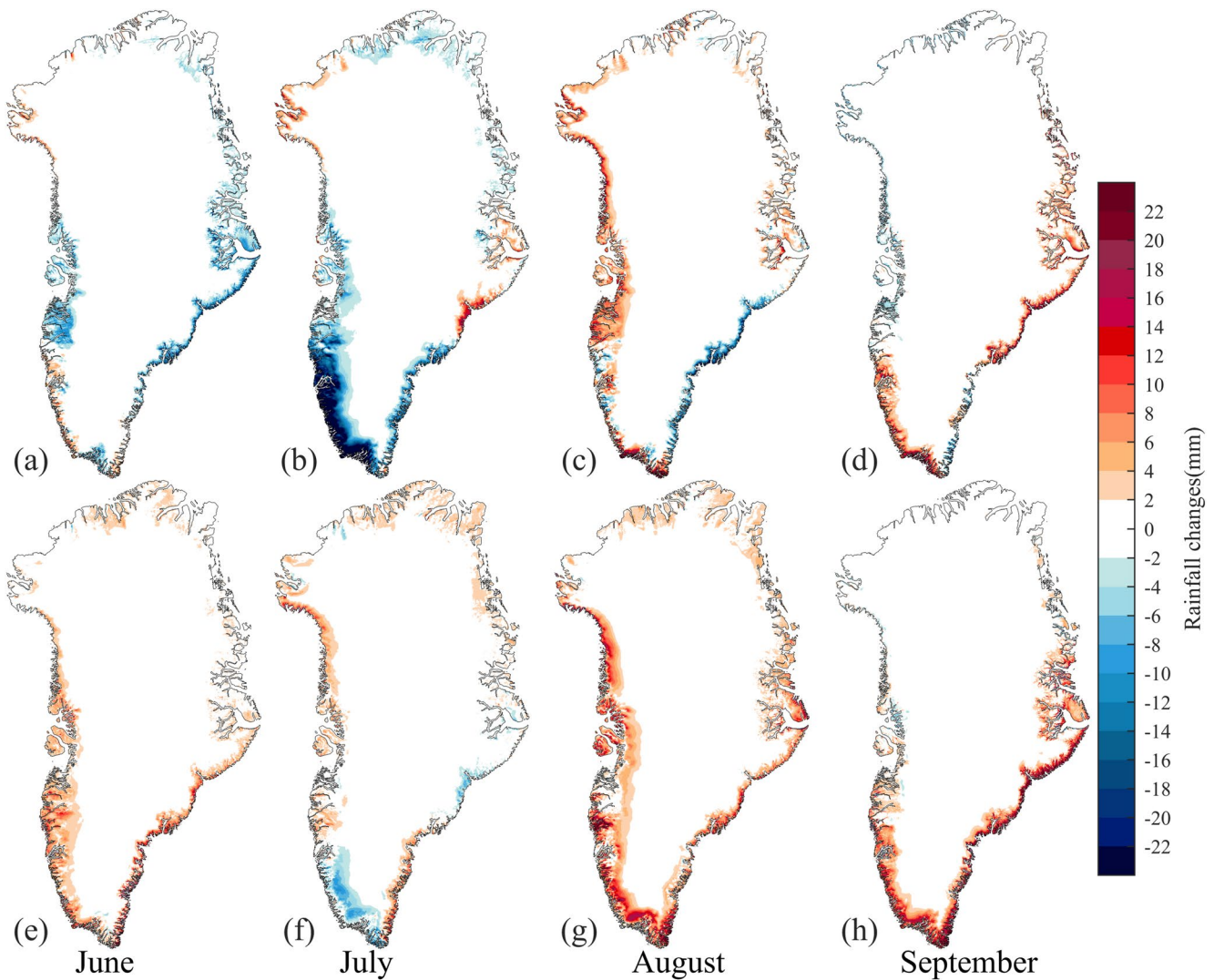
Figure 10. Partitioning of monthly rainfall changes (1991–2020 minus 1958–1990, in mm) as the contribution from total precipitation (amount effect, top row a, b, c, and d) and from changed rainfall fraction (bottom row, e, f, g, and h).

5. Conclusions

We present a daily, 1 km rainfall climatology of Greenland (1958–2020). It is based on statistical downscaling using the elevation dependence of snowfall fraction from a 5.5 km resolution regional climate model (RACMO2.3p2, 1958–2020). In general, rainfall and rainfall fraction decrease with increasing elevation, distance to coast and latitude in Greenland, but with large spatial deviations. The average (1958–2020) annual rainfall in Greenland is estimated to be 111.4 ± 11.2 Gt/year. The downscaled 1 km product better resolves the rainfall on low-lying and narrow glacier tongues and small ice caps (GIC). As a result, rainfall over GIC in the 1 km product is significantly greater (+124%) than previous estimates, for example, based on the 5.5 km product.

We found a pronounced shift in peak Greenland rainfall toward late summer. A large positive trend in rainfall (>40 mm/decade) during July and August is found in northwest Greenland mainly due to an increase in rainfall fraction (>3.5%/decade). Although most rain falls in the relatively mild south, with annual values locally exceeding 1,000 mm, the largest relative rainfall increase occurs in the colder northwest. Overall, during June, August, and September, the rainfall increases over GrIS, GIC, and tundra are predominantly caused by an increased rainfall fraction (52%–81%) rather than an increase in total precipitation ("amount effect"). Previous studies highlight the northwestern Greenland ice sheet as a regional hotspot of increasing runoff and dynamical mass loss (Mouginot et al., 2019; Wood et al., 2021), which may well be in part linked to increased rainfall. We show
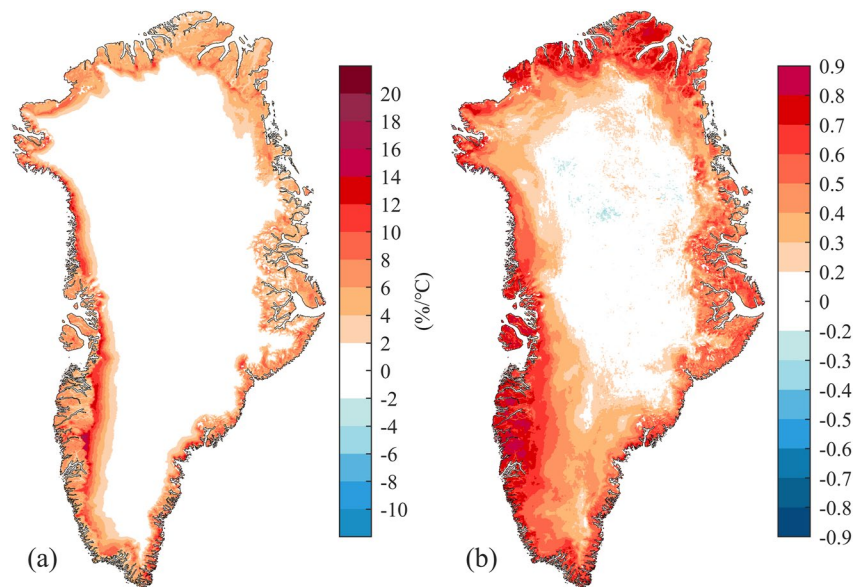
Figure 11. Regression slope (a) and correlation coefficient (b) during 1958–2020 June–September rainfall fraction and average 2 m temperature. The regression slope maps are scaled to show the rainfall fraction (%) change with 2 m temperature (°C) change.

that in summer, rainfall is closely linked to local near surface air temperature and that this dependency is strongest over the lower (ice sheet) slopes.

Data Availability Statement

Meteorological data set from the Danish Meteorological Institute (Cappelen, 2020) is available from https://www.dmi.dk/fileadmin/user_upload/Rapporter/TR/2020/DMIRep20-08.pdf; the RACMO2.3p2 model (Noël et al., 2016) and data analysis in Matlab software (version R2020a; Toby et al., 2015) are all openly available.

References

Bengtsson, L., Hodges, K. I., Koumoutsaris, S., Zahn, M., & Keenlyside, N. (2011). The changing atmospheric water cycle in Polar Regions in a warmer climate. *Tellus A: Dynamic Meteorology and Oceanography*, *63*(5), 907–920. https://doi.org/10.1111/j.1600-0870.2011.00534.x

Bintanja, R. (2018). The impact of Arctic warming on increased rainfall. *Scientific Reports*, *8*(1), 6–11. https://doi.org/10.1038/s41598-018-34450-3

Bintanja, R., & Andry, O. (2017). Towards a rain-dominated Arctic. *Nature Climate Change*, *7*(4), 263–267. https://doi.org/10.1038/nclimate3240

Bintanja, R., & Selten, F. M. (2014). Future increases in Arctic precipitation linked to local evaporation and sea-ice retreat. *Nature*, *509*(7501), 479–482. https://doi.org/10.1038/nature13259

Box, J. E., Bromwich, D. H., Veenhuis, B. A., Bai, L. S., Stroeve, J. C., Rogers, J. C., et al. (2006). Greenland ice sheet surface mass balance variability (1988–2004) from calibrated polar MM5 output. *Journal of Climate*, *19*(12), 2783–2800. https://doi.org/10.1175/jcli3738.1

Cappelen, J. (Ed.), Ed., (2020). Weather observations from Greenland 1958-2019 observation data with description[dataset]. Danish Meteorological Institute Report, 20-08. Retrieved From https://www.dmi.dk/fileadmin/user_upload/Rapporter/TR/2020/DMIRep20-08.pdf

Dou, T., Xiao, C., Liu, J., Han, W., Eicken, H., Mahoney, A. R., et al. (2019). A key factor initiating surface ablation of Arctic sea ice: Earlier and increasing liquid precipitation. *The Cryosphere*, *13*, 1233–1246. https://doi.org/10.5194/tc-2018-239

Doyle, S., Hubbard, A. L., van de Wal, R., Box, J. E., van As, D., Scharrer, K., et al. (2015). Amplified melt and flow of the Greenland ice sheet driven by late-summer cyclonic rainfall. *Nature Geoscience*, *8*, 647–653. https://doi.org/10.1038/ngeo2482

Endo, H., & Kitoh, A. (2014). Thermodynamic and dynamic effects on regional monsoon rainfall changes in a warmer climate. *Journal of Geophysical Research*, *41*(5), 1704–1710. https://doi.org/10.1002/2013GL059158

Ettema, J., van den Broeke, M. R., van Meijgaard, E., van de Berg, W. J., Bamber, J. L., Box, J. E., & Bales, R. C. (2009). Higher surface mass balance of the Greenland ice sheet revealed by high-resolution climate modeling. *Geophysical Research Letters*, *36*(12), D06116. https://doi.org/10.1029/2009GL038110

Fettweis, X., Franco, B., Tedesco, M., van Angelen, J. H., Lenaerts, J. T. M., van den Broeke, M. R., & Gallée, H. (2013). Estimating the Greenland ice sheet surface mass balance contribution to future sea level rise using the regional atmospheric climate model MAR. *The Cryosphere*, *7*(2), 469–489. https://doi.org/10.5194/tc-7-469-2013

Gadedjisso-Tossou, A., Adjegan, K. I., & Kablan, A. K. M. (2021). Rainfall and temperature trend analysis by Mann–Kendall test and significance for rainfed cereal yields in Northern Togo. *Science*, *3*(1), 17. https://doi.org/10.3390/sci3010017

Hanna, E., Cappelen, J., Fettweis, X., Mernild, S. H., Mote, T. L., Mottram, R., et al. (2021). Greenland surface air temperature changes from 1981 to 2019 and implications for ice-sheet melt and mass-balance change. *International Journal of Climatology*, *41*(S1), E1336–E1352. https://doi.org/10.1002/joc.6771

Hanna, E., Huybrechts, P., Steffen, K., Cappelen, J., Huff, R., Shuman, C., et al. (2008). Increased runoff from melt from the Greenland ice sheet: A response to global warming. *Journal of Climate*, *21*(2), 331–341. https://doi.org/10.1175/2007JCLI1964.1

Hanna, E., Jónsson, T., Ólafsson, J., & Valdimarsson, H. (2006). Icelandic coastal sea surface temperature records constructed: Putting the pulse on air–sea–climate interactions in the northern North Atlantic. Part I: Comparison with HadISST1 open-ocean surface temperatures and preliminary analysis of long-term patterns and anomalies of SSTs around Iceland. *Journal of Climate*, *19*, 5652–5666. https://doi.org/10.1175/JCLI3933.1

Hao, M., Luo, Y., Lin, Y. L., Zhao, Z. C., Wang, L., & Huang, J. B. (2019). Contribution of atmospheric moisture transport to winter Arctic warming. *International Journal of Climatology*, *39*(5), 2697–2710. https://doi.org/10.1002/joc.5982

Howat, I. M., Negrete, A., & Smith, B. E. (2014). The Greenland Ice Mapping Project (GIMP) land classification and surface elevation datasets. *The Cryosphere*, *8*(4), 1509–1518. https://doi.org/10.5194/tc-8-1509-2014

Huai, B. J., Van den Broeke, M. R., Reijmer, C. H., & Cappelen, J. (2021). Quantifying rainfall in Greenland: A combined observational and modeling approach. *Journal of Applied Meteorology and Climatology*, *60*, 1171–1188. https://doi.org/10.1175/JAMC-D-20-0284.1

Kopec, B. G., Feng, X., Michel, F. A., & Posmentier, E. S. (2016). Influence of sea ice on Arctic precipitation. *Proceedings of the National Academy of Sciences of the United States of America*, *113*(1), 46–51. https://doi.org/10.1073/pnas.1504633113

Lenaerts, J. T. M., Camron, M. D., Wyburn-Powell, C. R., & Kay, J. E. (2020). Present-day and future Greenland ice sheet precipitation frequency from CloudSat observations and the community Earth system model. *The Cryosphere*, *14*(7), 2253–2265. https://doi.org/10.5194/tc-14-2253-202

Lewis, G., Osterberg, E., Hawley, R., Marshall, H. P., Meehan, T., Graeter, K., et al. (2019). Recent precipitation decrease across the Western Greenland ice sheet percolation zone. *The Cryosphere*, *13*(11), 2797–2815. https://doi.org/10.5194/tc-13-2797-2019

McCrystall, M. R., Stroeve, J., Serreze, M., Forbes, B. C., & Screen, J. A. (2021). New climate models reveal faster and larger increases in Arctic precipitation than previously projected. *Nature Communications*, *12*(1), 6765. https://doi.org/10.1038/s41467-021-27031-y

Mernild, S. H., Hanna, E., McConnell, J. R., Sigl, M., Beckerman, A. P., Yde, J. C., et al. (2015). Greenland precipitation trends in a long-term instrumental climate context (1890–2012): Evaluation of coastal and ice core records. *International Journal of Climatology*, *35*(2), 303–320. https://doi.org/10.1002/joc.3986

Mouginot, J., Rignot, E., Bjørk, A. A., Van den Broeke, M. R., Millan, R., Morlighem, M., et al. (2019). Forty-six years of Greenland Ice Sheet mass balance from 1972 to 2018. *Proceedings of the National Academy of Sciences of the United States of America*, *116*(19), 9239–9244. https://doi.org/10.1073/pnas.1904242116

Niwano, M., Box, J. E., Wehrlé, A., Vandecrux, B., Colgan, W. T., & Cappelen, J. (2021). Rainfall on the Greenland ice sheet: Present-day climatology from a high-resolution non-hydrostatic polar regional climate model. *Geophysical Research Letters*, *48*(15), e2021GL092942. https://doi.org/10.1029/2021GL092942

Noël, B., Van Kampenhout, L., Van De Berg, W. J., Lenaerts, J., & van den Broeke, M. R. (2020). Brief communication: CESM2 climate forcing (1950–2014) yields realistic Greenland ice sheet surface mass balance. *The Cryosphere*, *14*(4), 1425–1435. https://doi.org/10.5194/tc-14-1425-2020

Noël, B., van de Berg, W. J., Lhermitte, S., & van den Broeke, M. R. (2019). Rapid ablation zone expansion amplifies north Greenland mass loss. *Science Advances*, *5*(9), eaaw0123. https://doi.org/10.1126/sciadv.aaw0123

Noël, B., van de Berg, W. J., Lhermitte, S., Wouters, B., Machguth, H., Howat, I., et al. (2017). A tipping point in refreezing accelerates mass loss of Greenland's glaciers and ice caps. *Nature Communications*, *8*(1), 1–8. https://doi.org/10.1038/ncomms14730

Noël, B., Van De Berg, W. J., Machguth, H., Lhermitte, S., Howat, I., Fettweis, F., & van den Broeke, M. R. (2016). A daily, 1 km resolution data set of downscaled Greenland ice sheet surface mass balance (1958–2015) [dataset]. The Cryosphere, *10*, 2361–2377. https://doi.org/10.5194/tc-10-2361-2016

Noël, B., van de Berg, W. J., van Meijgaard, E., Kuipers Munneke, P., Van de Wal, R. S. W., & Van den Broeke, M. R. (2015). Evaluation of the updated regional climate model RACMO2.3: Summer snowfall impact on the Greenland ice sheet. *The Cryosphere*, *9*(5), 1831–1844. https://doi.org/10.5194/tc-9-1831-2015

Noël, B., van de Berg, W. J., van Meijgaard, E., van de Wal, R. S. W., van den Broeke, M. R., Lenaerts, J. T. M., et al. (2018). Modelling the climate and surface mass balance of polarice sheets using RACMO2-Part 1: Greenland (1958–2016). *The Cryosphere*, *12*(3), 811–831. https://doi.org/10.5194/tc-12-811-2018

Oltmanns, M., Straneo, F., & Tedesco, M. (2019). Increased Greenland melt triggered by large-scale, year-round cyclonic moisture intrusions. *The Cryosphere*, *13*(3), 815–825. https://doi.org/10.5194/tc-13-815-2019

Pan, S. F., Dou, T. F., Lin, L., Yang, J., Zhang, F., Duan, M. K., et al. (2021). Larger sensitivity of Arctic precipitation phase to aerosol than greenhouse gas forcing. *Geophysical Research Letters*, *47*(23). e2020GL090452. https://doi.org/10.1029/2020GL090452

Rastner, P., Bolch, T., Mölg, N., Machguth, H., Le Bris, R., & Paul, F. (2012). The first complete inventory of the local glaciers and ice caps on Greenland. *The Cryosphere*, *6*, 1483–1495. https://doi.org/10.5194/tc-6-1483-2012

Schuenemann, K. C., & Cassano, J. J. (2010). Changes in synoptic weather patterns and Greenland precipitation in the 20th and 21st centuries: 2. Analysis of 21st century atmospheric changes using self-organizing maps. *Journal of Geophysical Research*, *115*(D5), D05108. https://doi.org/10.1029/2009JD011706

Screen, J. A., & Simmonds, I. (2012). Declining summer snowfall in the Arctic: Causes, impacts and feedbacks. *Climate Dynamics*, *38*(11–12), 2243–2256. https://doi.org/10.1007/s00382-011-1105-2

Serreze, M. C., Barrett, A. P., Stroeve, J. C., Kindig, D. N., & Holland, M. M. (2009). The emergence of surface-based Arctic amplification. *The Cryosphere*, *3*(1), 11–19. https://doi.org/10.5194/tc-3-11-2009

Shannon, S. R., Payne, A. J., Bartholomew, I. D., van den Broeke, M. R., Edwards, T. L., Fettweis, X., et al. (2013). Enhanced basal lubrication and the contribution of the Greenland ice sheet to future sea-level rise. *Proceedings of the National Academy of Sciences of the United States of America*, *110*(35), 14156–14161. https://doi.org/10.1073/pnas.1212647110

Shepherd, A., Ivins, E., Rignot, E., Smith, B., & Wuite, J. (2020). Mass balance of the Greenland ice sheet from 1992 to 2018. *Nature*, *579*(7798), 233–239. https://doi.org/10.1038/s41586-019-1855-2

Shepherd, A., & Wingham, D. (2007). Recent sea-level contributions of the Antarctic and Greenland ice sheets. *Science*, *315*(5818), 1529–1532. https://doi.org/10.1126/science.1136776

Steffen, K., & Box, J. E. (2001). Surface climatology of the Greenland ice sheet: Greenland climate network 1995-1999. *Journal of Geophysical Research*, *106*(D24), 33951–33964. https://doi.org/10.1029/2001JD900161

Tedesco, M., Mote, T., Fettweis, X., Hanna, E., Jeyaratnam, J., Booth, J. F., et al. (2016). Arctic cut-off high drives the poleward shift of a new Greenland melting record. *Nature Communications*, *7*(1), 11723. https://doi.org/10.1038/ncomms11723

The IMBIE team. (2020). Mass balance of the Greenland ice sheet from 1992 to 2018. *Nature*, *579*(7798), 233–239. https://doi.org/10.1038/s41586-019-1855-2

Toby, A. R., Zurita Milla, R., & Schwartz, M. D., (2015). A Matlab toolbox for calculating spring indices from daily meteorological data [Software]. Computers & Geosciences, *83*, 46–53. https://doi.org/10.1016/j.cageo.2015.06.015

Van Meijgaard, E., Van Ulft, L. H., Van de Berg, W. J., Bosveld, F. C., Van den Hurk, B. J. J. M., Lenderink, G., & Siebesma, A. P. (2008). *The KNMI regional atmospheric climate model RACMO version 2.1*. Technical Report 302. KNMI.

Van Wessem, J. M., Reijmer, C. H., Lenaerts, J. T. M., Van de Berg, W. J., Van den Broeke, M. R., & Van Meijgaard, E. (2014). Updated cloud physics in a regional atmospheric climate model improves the modelled surface energy balance of Antarctica. *The Cryosphere*, *8*(1), 125–135. https://doi.org/10.5194/tc-8-125-2014

Van den Broeke, M. R., Enderlin, E. M., Howat, I. M., Kuipers Munneke, P., Noël, B. P. Y., van de Berg, W. J., et al. (2016). On the recent contribution of the Greenland ice sheet to sea level change. *The Cryosphere*, *10*(5), 1933–1946. https://doi.org/10.5194/tc-10-1933-2016

Vihma, T., Screen, J., Tjernström, M., Newton, B., Zhang, X. D., Popova, V., et al. (2016). The atmospheric role in the arctic water cycle: A review on processes, past and future changes, and their impacts. *Journal of Geophysical Research*, *121*(3), 586–620. https://doi.org/10.1002/2015JG.003132

Wang, S., Nath, D., Chen, W., & Wang, L. (2019). Recent strengthening of Greenland blocking drives summertime surface warming over northern Canada and eastern Siberia. *Journal of Climate*, *32*(11), 3263–3278. https://doi.org/10.1175/JCLI-D-18-0410.1

Wood, M., Rignot, E., Fenty, I., An, L., Bjørk, A., Van den Broeke, M. R., et al. (2021). Ocean forcing drives glacier retreat in Greenland. *Science Advances*, *7*(1), eaba7282. https://doi.org/10.1126/sciadv.aba7282

Woods, C., Caballero, R., & Svensson, G. (2013). Large-scale circulation associated with moisture intrusions into the Arctic during winter. *Geophysical Research Letters*, *40*(17), 4717–4721. https://doi.org/10.1002/grl.50912

Yang, D., Ishida, S., Goodison, B. E., & Gunther, T. (1999). Bias correction of daily precipitation measurements for Greenland. *Journal of Geophysical Research*, *104*(D6), 6171–6181. https://doi.org/10.1029/1998JD.200110

Zhang, Q., Huai, B. J., Van Den Broeke, M. R., Cappelen, J., Ding, M. H., Wang, Y. T., & Sun, W. J. (2022). Temporal and spatial variability in contemporary Greenland warming (1958–2020). *Journal of Climate*, *1*(9), 2755–2767. https://doi.org/10.1175/JCLI-D-21-0313.1

Zwally, H. J., Abdalati, W., Herring, T., Larsen, K., Saba, J., & Steffen, K. (2002). Surface melt-induced acceleration of Greenland ice-sheet flow. *Science*, *297*(5579), 218–222. https://doi.org/10.1126/science.1072708

Zwally, H. J., & Giovinetto, M. B. (2001). Balance mass flux and ice velocity across the equilibrium line in drainage systems of Greenland. *Journal of Geophysical Research*, *106*(D24), 33717–33728. https://doi.org/10.1029/2001JD900120